Nanoscale

COMMUNICATION

View Article Online
View Journal | View Issue

Cite this: *Nanoscale*, 2020, **12**, 10491

Received 28th January 2020,
Accepted 2nd May 2020

DOI: 10.1039/d0nr00755b

rsc.li/nanoscale

Vertically-oriented MoS_2 nanosheets for nonlinear optical devices†

M. Bolhuis, J. Hernandez-Rueda, S. E. van Heijst, M. Tinoco Rivas, ‡ L. Kuipers and S. Conesa-Boj *

Transition metal dichalcogenides such as MoS_2 represent promising candidates for building blocks of ultra-thin nanophotonic devices. For such applications, vertically-oriented MoS_2 (v-MoS_2) nanosheets could be advantageous as compared to conventional horizontal MoS_2 (h-MoS_2) given that their inherent broken symmetry would favor an enhanced nonlinear response. However, the current lack of a controllable and reproducible fabrication strategy for v-MoS_2 limits the exploration of this potential. Here we present a systematic study of the growth of v-MoS_2 nanosheets based on the sulfurization of a pre-deposited Mo–metal seed layer. We demonstrate that the sulfurization process at high temperatures is driven by the diffusion of sulfur from the vapor–solid interface to the Mo seed layer. Furthermore, we verify an enhanced nonlinear response in the resulting v-MoS_2 nanostructures as compared to their horizontal counterparts. Our results represent a stepping stone towards the fabrication of low-dimensional TMD-based nanostructures for versatile nonlinear nanophotonic devices.

Introduction

Two-dimensional (2D) materials such as transition metal dichalcogenides (TMDs) have been extensively exploited for a wide range of applications including optoelectronics devices[1,2] and catalysis[3] among others. Specifically, these materials exhibit numerous remarkable electronic and optical properties thanks to their broken inversion symmetry.[4–6] Significant attention has been recently devoted to their nonlinear optical response,[7–9] which makes TMDs ideal building blocks for ultra-thin[10] nonlinear photonic devices.[11]

Such nonlinear optical effects have been demonstrated in horizontal MoS_2 (h-MoS_2) monolayers, displaying a marked dependence on the specific crystalline symmetry and orientation.[12] For instance, a nonlinear optical response has been reported at the atomic edges of h-MoS_2 crystals, where translation symmetry is broken.[13] These findings suggest that vertically-oriented MoS_2 (v-MoS_2) nanosheets, a configuration that maximizes the number of exposed edge sites, could represent a promising platform to enhance the second-order nonlinear response and realize a novel candidate for the building blocks of high efficiency nanophotonic devices.

On the one hand, significant progress has been achieved in the understanding of the growth dynamics of horizontal MoS_2. Different fabrication methods have been employed, such as chemical vapor deposition (CVD) techniques,[14,15] the direct sulfurization of a pre-deposited molybdenum (Mo) seed layer,[16,17] the solvothermal/hydrothermal approach,[18] and by using a vapor phase reaction with MoO_3.[19,20]

On the other hand, the growth mechanism of its vertical counterpart, v-MoS_2, remains still poorly understood. Several attempts at explaining the growth of vertically-oriented MoS_2 nanostructures have been put forward. For instance, in the context of growth strategies based on the sulfurization of a pre-existing Mo–metal layer,[21] it has been shown that a low reaction temperature of 550 °C results into v-MoS_2 with the kinetically-controlled growth being diffusion limited. Furthermore, it has been reported that the orientation of the resulting MoS_2 layers with respect to the substrate is sensitive to the thickness of the Mo–metal layer.[22] Specifically, thicker and more uniform Mo–metal seed layers lead to a higher fraction of v-MoS_2 layers. Additionally, theoretical models have been also constructed aiming to describe the synthesis of vertically-oriented MoS_2 based on the solid-vapor reaction,[21–24] though most of these predictions remain to be verified.

Given this state of affairs, achieving further progress towards a controllable and reproducible fabrication strategy for v-MoS_2 requires detailed studies of the associated growth mechanisms. Here we present a systematic investigation of the

Kavli Institute of Nanoscience, Delft University of Technology, 2628CJ Delft, The Netherlands. E-mail: s.conesaboj@tudelft.nl

†Electronic supplementary information (ESI) available: Additional information about the synthesis and characterization of vertically-oriented MoS_2 nanosheets. See DOI: 10.1039/d0nr00755b

‡Present address: ICTS – Centro Nacional de Microscopía Electrónica, Universidad Complutense, 28040, Spain.

growth mechanism of vertical MoS_2 nanosheets based on the sulfurization of a pre-deposited Mo–metal seed layer. Thanks to an extensive structural cross-section characterization by means of transmission electron microscopy (TEM), we demonstrate that the sulfurization mechanism for temperatures between 600 and 700 °C proceeds *via* diffusion. These findings imply that during the sulfur reaction the growth propagates from the vapor–solid interface inwards into the Mo seed layer. In addition, we investigate the prospects of the resulting v-MoS_2 nanostructures for nonlinear optical applications. We verify an enhanced nonlinear response as compared to their h-MoS_2 counterparts, confirmed by the observation of second-harmonic generation and sum-frequency generation.

Our results provide a stepping stone towards the large-scale fabrication of high-quality v-MoS_2 nanosheets, and represent a crucial step in a program aimed at designing and fabricating low-dimensional nanostructures for the development of efficient and versatile nonlinear optical devices based on 2D materials.

Results and discussion

A two-step process was used for synthesizing the vertically-oriented MoS_2 nanosheets by means of the sulfurization of a pre-deposited Mo–metal layer. A thick Mo seed layer of 700 nm was chosen in order to be able to ascertain the dependence on the reaction time and the sulfurization depth. The sulfurization process was carried out inside a three-zone hot-wall horizontal tube. Before and during the sulfurization, an Argon gas flow was used to prevent any possible oxidation as well as a carrier to transport the Sulphur vapor phase to the substrate. Further details about the growth process are described in the ESI.†

The orientation of the resulting MoS_2 nanosheets was investigated as a function of the reaction temperature. For these studies, we considered several growth temperatures in the range between 500 °C and 700 °C. We now highlight the results obtained for the two limiting cases corresponding to temperatures of 500 °C and 700 °C.

Fig. 1a and b display top-view scanning electron microscopy (SEM) images of the sulfurized Mo–metal layer at 500 and 700 °C respectively. One observes marked differences in the morphology between the results obtained in the two growths. While the vertical nature of the MoS_2 nanosheets grown at a temperature of 500 °C is unambiguous from the SEM image (Fig. 1a), the same inspection is less conclusive for the sample grown at 700 °C, whose surface exhibits a granular-like aspect (Fig. 1b).

Fig. 1c and d depict Raman spectroscopy measurements taken in the samples grown at 500 and 700 °C, respectively. These Raman spectra are dominated by the in-plane E^1_{2g} and the out-of-plane A_{1g} Raman modes. The appearance and position of these peaks is consistent with a trigonal prismatic (2H-MoS_2) crystal phase, further confirming the successful MoS_2 growth.[25]

Interestingly, we find that for the sample grown at 500 (700) °C the ratio of intensities between the A_{1g} and E^1_{2g} peaks increases by a factor 2 (3) as compared to regular MoS_2 flakes, where the two peaks exhibit comparable intensities.[22] Given

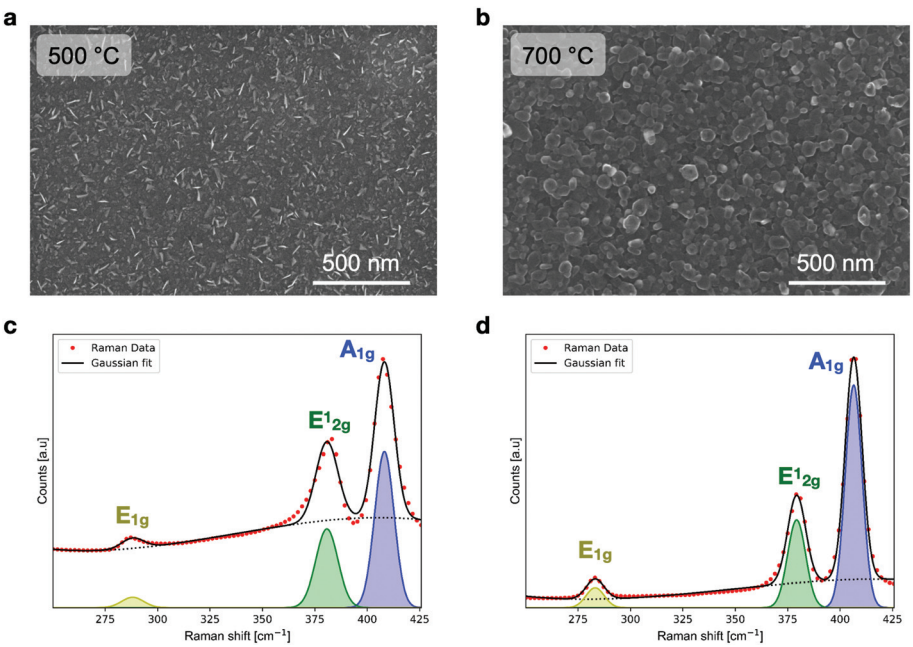

Fig. 1 (a) and (b) Top-view SEM images of the surface of the samples sulfurized at 500 and 700 °C, respectively. (c) and (d) The associated Raman spectra, where the two main Raman modes (A_{1g} and E^1_{2g}) are visible along with the smaller E_{1g} mode. The similarities between the two spectra suggest the vertical orientation of the MoS_2 nanosheets in the samples grown at both temperatures.

that the A_{1g} and E^1_{2g} Raman peaks are associated respectively with the out-of-plane and in-plane vibration modes, these results suggest that our specimens exhibit the presence of v-MoS_2 nanosheets in the samples grown at both temperatures, therefore indicating a higher density of exposed edges.

Furthermore, in Fig. 1c (1d) a third peak located at 287 (283) cm^{-1} and associated to the E_{1g} Raman mode is also observed. This mode is forbidden in backscattering experiments,[26] which implies that it should not be observed when the incident laser beam is perpendicular to the basal plane, as happens for horizontal MoS_2. The presence of the E_{1g} mode thus indicates that the laser beam is no longer perpendicular to the incident (basal) plane, providing a further confirmation of the presence of vertically-oriented (with respect to the substrate) MoS_2 nanosheets in both samples.

To investigate the orientation of the grown MoS_2, we further complement this surface analysis with a cross-section study performed by focus ion beam (FIB) followed by SEM inspection. For the sample grown at 500 °C (Fig. 2a), the thickness of the original Mo seed layer (700 nm) remains mostly unaffected after sulfurization. However, for the sample grown at 700 °C (Fig. 2b), the Mo seed layer is close to being fully sulfurized. From the cross-section SEM image, one observes that the original thickness of the Mo–metal layer has been reduced down to a length of 200 nm, with the rest of the Mo layer sulfurized into MoS_2. In this specific case, the final sulfurized layer has a length of 1.95 μm, representing a factor of around three increase as compared to the thickness of the initial Mo layer.

From these experimental results, one can therefore distinguish two distinctive dynamics for the growth of the v-MoS_2 nanosheets. On the one hand, at 500 °C, the sulfur only reacts on the immediate Mo seed layer surface, leading to vertically-standing MoS_2 as can be observed in the top-view SEM image in Fig. 1a. On the other hand, at 700 °C, the sulfur diffuses through the Mo seed layer by consuming it and forming v-MoS_2 layers.

To investigate the crystalline quality of the vertical MoS_2 grown at 700 °C, we have produced a cross-section sample using FIB and then analyzed it by means of transmission electron microscopy (TEM). The three different contrasts observed in Fig. 3a reveal the sequence MoS_2, Mo–metal layer, and Silicon. The high-resolution TEM (HRTEM) measurements performed at the MoS_2/Mo interface (Fig. 3b) indicate that the MoS_2 grows vertically with respect to the Mo seed layer. The distance between two neighboring MoS_2 layers was measured to be about 0.65 nm (Fig. 3c), consistent with previous results in the literature.[27] Energy dispersive X-ray spectroscopy (EDX) measurements along the length of the whole cross-section (Fig. 3d) provide clear evidence of the sulfur diffusion into the Mo seed layer that results into the growth of the vertically-oriented MoS_2 nanosheets.

Growth mechanism of vertically-oriented MoS_2 nanosheets at 700 °C

In order to further elucidate the sulfurization mechanism of the v-MoS_2 at 700 °C, we have sulfurized for different times sample containing each 700 nm of Mo seed layer. Subsequently, we prepared with FIB cross-sections lamellas for TEM and EDX inspection that allowed us to determine the thicknesses of the MoS_2 layer and of the consumed Mo. We have only considered reactions times equal to and larger than 15 min, in a way that the Mo seed layer will be always completely sulfurized, see Fig. S5.† In Fig. 4a we display the value of the consumed Mo seed layer as a function of the reaction time. These measurements are fitted to a model of the form $z = K(t - t_0)^n$, with z and t are the thickness of the consumed Mo seed layer and the reaction time respectively. The best-fit value for the growth exponent n is found to be 0.48. The fact that n is very close to 1/2 is consistent with a sulfurization process dominated by the diffusion mechanism.

Since the growth exponent is essentially 0.5, we can use the relation $z_{dif} = 2\sqrt{Dt}$ to extract from the data the diffusion coefficient of sulfur within the Mo seed layer. The best-fit value for D is calculated to be 20.7 $nm^2\ s^{-1}$, similar to the diffusion coefficients measured for sulfur in other metals.[28]

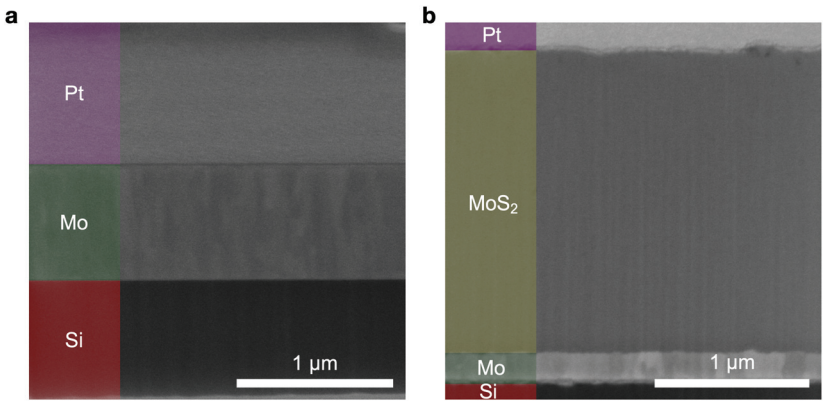

Fig. 2 (a) and (b) SEM images of the FIB cross-sections corresponding to the samples shown in Fig. 1a and b. In (a), the sample grown at 500 °C, we observe three distinctive regions with different contrasts, associated to the protective Pt layer (magenta), the Mo seed layer (green), and the Si substrate (red). Note that in this case the presence of MoS_2 is restricted to the surface of the sample. In (b), grown at 700 °C, the four regions are associated to the protective Pt (magenta), the MoS_2 layer with vertical nanosheets (yellow), the Mo seed layer (green), and the Si substrate (red).

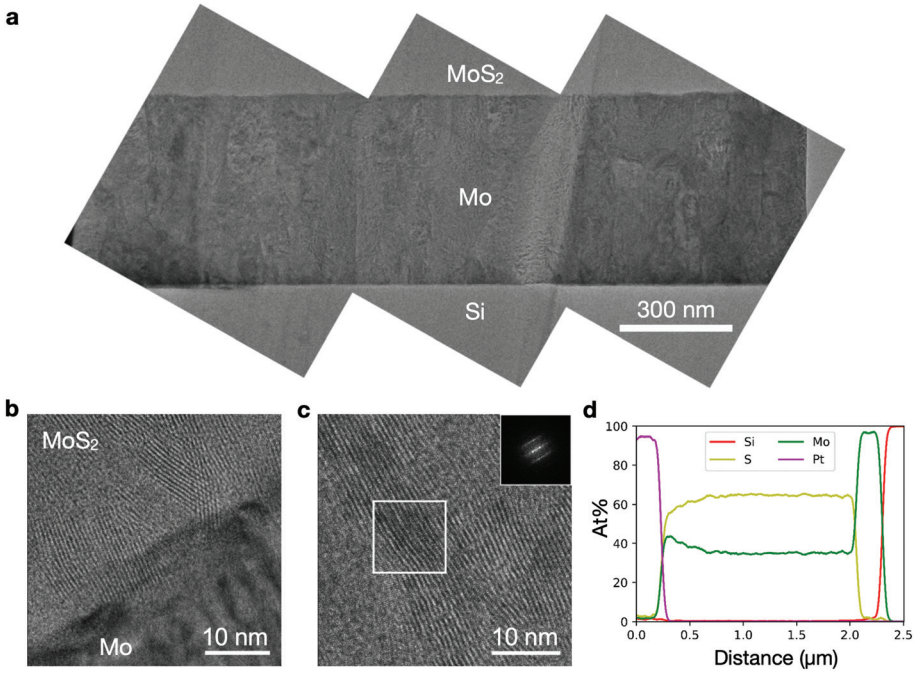

Fig. 3 (a) Reconstructed low-magnification bright-field TEM image of a sample sulfurized at 700 °C, displaying the Mo seed layer sandwiched between v-MoS_2 on the top and the Si substrate on the bottom. (b) HRTEM image of the interface region showing how the v-MoS_2 nanosheets arise from the Mo–metal layer. (c) HRTEM image of a region containing only v-MoS_2 nanosheets, together with the FFT calculated in the area highlighted with a white square in the inset. (d) EDX line scan of a sample sulfurized for 1 hour at 700 °C indicating its elemental composition.

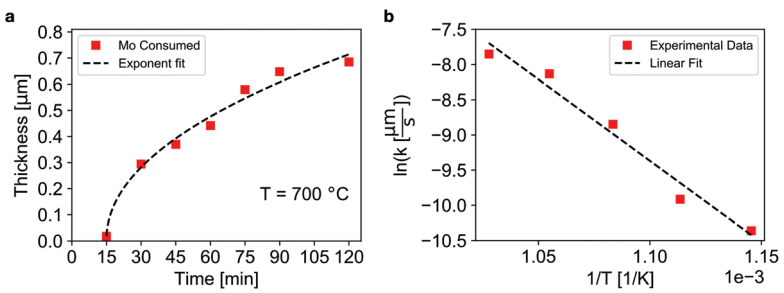

Fig. 4 (a) The thicknesses of the consumed Mo–metal layer as a function of the reaction time for the sample grown at 700 °C. The dotted line corresponds to a model fit of the form $z = K(t - t_0)^n$. The best-fit growth exponent is found to be $n = 0.48$, very close to the $n = 0.5$ expected for a diffusion-driven process. (b) An Arrhenius diagram where the logarithm of the rate constant k is represented as a function of the inverse of the reaction temperature. The linear fit to the data allows us to determine the activation energy required to sulfurize the Mo seed layer.

Our findings therefore confirm that the reaction is driven by the diffusion of the sulfur and that the consumption of sulfur takes place predominantly at the boundary between the Mo seed layer and the grown v-MoS_2 layers. These results are consistent with theoretical models of the diffusion-reaction growth proposed for the synthesis of vertically-oriented MoS_2.[29]

From the HR-TEM cross-section lamella analysis (Fig. S4†) we also found an orientation-disordered region extending from the surface to the first 20 nanometers, where both vertical and horizontal MoS_2 nanosheets are present. The reaction mechanism in this initial region appears to be self-limited,[29] but then from this point onwards the growth front results into v-MoS_2 being dominated by the diffusion kinetics of sulfur, as discussed above.

The influence of the temperature on the rate of the consumed Mo seed layer was also examined in the range between 600 and 700 °C. The lower range of this interval corresponds to the minimum temperature required to initiate the diffusion of the sulfur within the Mo seed layer.[21] A fixed reaction time of 30 min was adopted in these experiments. Fig. 4b highlights the effect of the rate of the MoS_2 thickness growth as a function of the reaction temperature. The experimental Arrhenius plot can be fitted very well by a straight line to determine the activation energy E_A, which turns out to be 192.44 kJ mol^{-1}. These findings provide additional evidence that the sulfur

diffuses in the range between 600 and 700 °C through the Mo seed layer, leading to the phase transformation into vertically-oriented MoS_2 nanosheets.

Nonlinear optical effects in vertical-oriented MoS_2 nanosheets

As mentioned above, TMD materials have generated ample attention because of their nonlinear optical response.[7] In particular, second and third-order nonlinear optical processes have recently been demonstrated in few-layer MoS_2 flakes. Second-harmonic (SHG) and sum-frequency generation (SFG) have been shown to be more efficiently generated in thin MoS_2 flakes with a few atomic layers.[30,31] The intensity of both processes exponentially increases when decreasing the number of layers, thus revealing MoS_2 monolayers to be the most efficient thickness in order to generate second-order processes. Moreover, due to inversion symmetry breaking, only odd-layered MoS_2 flakes present second-order processes, (*i.e.* MoS_2 layered semiconductors have vanishing $\chi^{(2)}$ due to symmetry when the number of layers is even). In contrast, third-order processes, such as four-wave mixing (FWM), gradually increase their intensity with increasing number of layers (reaching saturation for a certain thickness) irrespective of their parity.

It is also worth noting that the study of nondegenerate optical processes in MoS_2 flakes using multi-color multiphonon spectroscopy is very limited in the literature.[7,12]

Here we use multiphoton spectroscopy to explore the nonlinear optical response of the synthesized vertical MoS_2 nanosheets reported in this work, and compare the results with those of their h-MoS_2 counterparts. Fig. 5a depicts the spectra of the nonlinear emission when excited with a laser pulse at 776 nm (blue line) and with two synchronized laser pulses at 776 nm and 1210 nm (red line). The labels indicate the nonlinear mechanisms that originate the emission at each spectral peak. The spectra in Fig. 5a illustrate all the above-mentioned processes. In order to benchmark the response of the v-MoS_2 nanosheets in Fig. 5a, we also measured the nonlinear emission of the horizontally-oriented case. Fig. 5b shows the spectra collected upon laser illumination with a single 776 nm beam (blue line) and both beams at 776 nm and 1210 nm (red line). Although both MoS_2 geometries exhibit the same emission peaks (except SHG_2), it is clear that vertically-oriented MoS_2 nanosheets favor second-order processes (*i.e.* SFG in Fig. 5a) over third-order processes (*i.e.* THG and FWM in Fig. 5a). In contrast, the horizontal configuration shows the opposite trend where third-order processes dominate and second-order processes are three orders of magnitude smaller due to inversion symmetry, in agreement with previous results in the literature.[12,32]

By using the intensity of the spectral peaks for SFG and SHG along with the power of the excitation beams, one can estimate the relative ratio of the nonlinear susceptibility.[7,33] The relevant formulae related to second harmonic generation and sum frequency generation are provided in the ESI-G.† The second-order susceptibility ratios between the vertical and horizontal geometries extracted from SHG and SFG turn out to be $\chi_V^{(2)}/\chi_H^{(2)}|_{SHG} = 22.9 \pm 1.5$ and $\chi_V^{(2)}/\chi_H^{(2)}|_{SFG} = 24.7 \pm 1.0$, respectively. These results indicate that vertically-oriented MoS_2 nanosheets significantly favor second-order nonlinear processes as compared to their horizontal counterparts. As mentioned above, this enhancement can be traced back to the effects of inversion symmetry breaking at the exposed edges of the nanosheets.

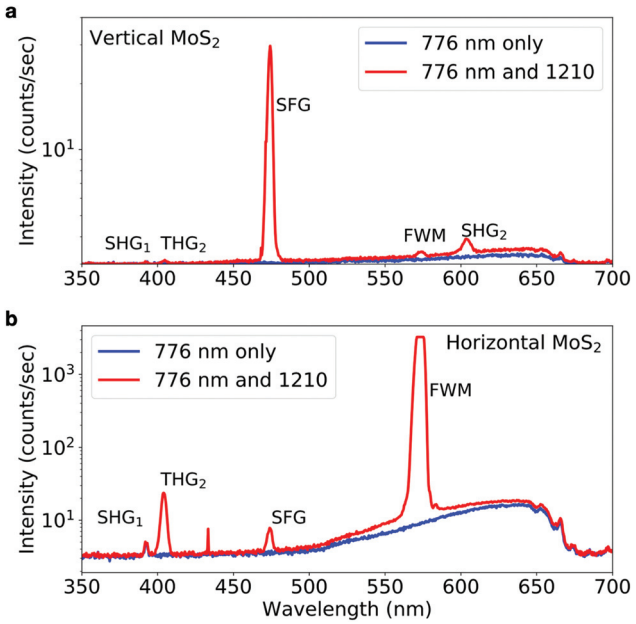

Fig. 5 Spectra from a vertical (a) and horizontal (b) MoS_2 nanosheets simultaneously illuminated with ultrashort laser pulses at 776 nm and 1210 nm. The labels next to each peak indicate the corresponding nonlinear mechanisms that mediate each emission. The repletion rate of the laser during the experiments was 80 MHz and the pulse duration 230 fs. The energy of the laser pulses used in (a) were 7.5 pJ at 776 nm and 15.4 pJ at 1210 nm in (b) 380 pJ at 776 nm and 48 pJ at 1210 nm. Note that we present the spectra in counts per second by using integration times of (a) 150 seconds and (b) 20 seconds.

Conclusions

In this work we have reported the controllable and reproducible fabrication of vertically-oriented MoS_2 nanosheets. We have demonstrated that the phase transformation from Mo seed layers to vertically-oriented 2H-MoS_2 nanosheets can be achieved by means of reacting the pre-deposited Mo–metal layer with sulfur at relatively high temperatures, in the range between 600 and 700 °C. Following a systematic characterization analysis of these v-MoS_2 nanosheets using TEM and EDX, we have established that in this range of temperatures the sulfurization mechanism proceeds *via* diffusion.

Furthermore, we have investigated the nonlinear optical response of the resulting v-MoS_2 nanostructures, including second-harmonic generation, and found an enhanced second-order nonlinear response as compared to the h-MoS_2 case. The latter property could be explained by the effects of inversion symmetry breaking at the exposed edges of the nanosheets.

Our findings therefore represent a stepping stone towards the fabrication of low-dimensional TMD-based nanostructures for versatile nonlinear nanophotonic devices. This above-mentioned nonlinear property combined with the versatility of the synthesis method have the potential to create flexible, large area, nonlinear photonic devices based on a wide array of layered materials.

Methods

Sample preparation

A two-step process was used for synthesizing the vertically-oriented MoS_2 nanosheets. First, a 700 nm-thick Mo seed layer was pre-deposited on a Si/SiO_2 wafer using magnetron sputtering. The sulfurization was carried out in a gradient tube furnace from Carbolite Gero. Note that Argon gas was used as a carrier gas. The Ar flow was set up 150 sccm for all the syntheses (see Fig. S2†). This Mo seed layer was placed in the middle zone and gradually heated up to the reaction temperature. Once the sample reached the reaction temperature, 400 mg of sulfur was heated to 220 °C (see Fig. S1–S3†). The sulfur was placed upstream from the sample. Further details on the synthesis can be found in the ESI.†

Characterization techniques

Transmission electron microscopy (TEM) measurements. TEM and energy-dispersive X-ray spectroscopy were carried out in a Titan Cube microscope operated at 300 kV. Its spatial resolution at Scherzer defocus conditions is 0.08 nm in the High-resolution TEM mode, whilst the resolution is around 0.19 nm in the High-Angle Annular Dark-Field Scanning Transmission Electron Microscopy (HAADF-STEM). Cross-section TEM lamellas were fabricated using a FEI Helios G4 CX™ dual beam system.

Raman spectroscopy. Raman spectroscopy was performed using a Renishaw InVia Reflex™ confocal Raman microscope. The wavelength of the exiting laser was 514 nm, and a 1800 l mm^{-1} grating was used resulting in a spectral resolution of around 1 cm^{-1}.

Optical measurements. For the nonlinear optical measurements, the specimen was prepared by means of the ultramicrotomy technique.[34] See ESI-E† for more details. The specimen was illuminated with two synchronized laser pulses at λ_1 = 776 nm and λ_2 = 1210 nm that were temporally and spatially overlapped. The laser pulses were generated by a femtosecond laser oscillator (Tsunami, Spectra-Physics) and an optical parametric oscillator (OPAL, Spectra-Physics). Both laser beams were focused onto the sample using a microscope objective (Olympus UP-LSAPO 40×/0.95), which also collects the emitted light originated through the nonlinear laser-v-MoS_2-nanosheets interaction. The collected light was filtered and imaged onto the slit of a spectrometer (PI, Spectra Pro 2300I). In these measurements the second-order susceptibility $\chi^{(2)}$ gives rise to the second-harmonic generation (SHG) and the sum-frequency generation (SFG) at $2\omega_1$, $2\omega_2$ and $\omega_1 + \omega_2$. The third-order susceptibility $\chi^{(3)}$ mediates the generation of nonlinear polarization $P^{(3)}$, resulting in third-harmonic generation (THG) and four-wave mixing (FWM) at $3\omega_2$ and $2\omega_1 - \omega_2$, respectively.

Conflicts of interest

There are no conflicts to declare.

Acknowledgements

M. B., S. E. v. H., and S. C.-B. acknowledge financial support from ERC through the Starting Grant "TESLA" grant agreement no. 805021. M. T. R. acknowledges support from the Netherlands Organizational for Scientific Research (NWO) through the Nanofront program. The authors L. K. and J. H.-R. acknowledge funding in the framework of FP7 Ideas: European Research Council (ERC 340438-CONSTANS).

References

1 L. Britnell, R. M. Ribeiro, A. Eckmann, R. Jalil, B. D. Belle, A. Mishchenko, Y.-J. Kim, R. V. Gorbachev, T. Georgiou, S. V. Morozov, A. N. Grigorenko, A. K. Geim, C. Casiraghi, A. H. Castro Neto and K. S. Novoselov, Strong light-matter interactions in heterostructures of atomically thin films, *Science*, 2013, **340**, 1311–1314.
2 C.-H. Lee, G.-H. Lee, A. M. van der Zande, W. Chen, Y. Li, M. Han, X. Cui, G. Arefe, C. Nuckolls, T. F. Heinz, J. Guo, J. Hone and P. Kim, Atomically thin p-n junctions with van der Waals heterointerfaces, *Nat. Nanotechnol.*, 2014, **9**, 676–681.
3 T. F. Jaramillo, K. P. Jørgensen, J. Bonde, J. H. Nielsen, S. Horch and I. Chorkendorff, Identification of active edge sites for electrochemical H_2 evolution from MoS_2 nanocatalysis, *Science*, 2007, **317**, 100–102.
4 M. Tinoco, L. Maduro and S. Conesa-Boj, Metallic edge states in zig-zag vertically-oriented MoS_2 nanowalls, *Sci. Rep.*, 2019, **9**, 15602.
5 S.-H. Gong, F. Alpeggian, B. Sciacca, E. C. Garnett and L. Kuipers, Nanoscale chirial valley-photon interface through optical spin-orbit coupling, *Science*, 2018, **359**, 443–447.
6 Z. Sun, A. Martinez and F. Wang, Optical modulators with 2D layered materials, *Nat. Photonics*, 2016, **10**, 227–238.
7 T. Jakubczyk, V. Delmonte, M. Koperski, K. Nogajewski, C. Faugeras, W. Langbein, M. Potemski and J. Kasprzak, Radiatively Limited Dephasing and Exciton Dynamics in $MoSe_2$ Monolayers Revealed with Four-Wave Mixing Microscopy, *Nano Lett.*, 2016, **16**, 5333–5339.
8 A. Autere, H. Jussila, Y. Dai, Y. Wang, H. Lipsanen and Z. Sun, Nonlinear Optics with 2D Layered Materials, *Adv. Mater.*, 2018, **30**, 1705963–17059678.

9 X. Zhang, S. Zhang, Y. Xie, J. Huang, L. Wang, Y. Cui and J. Wang, Tailoring the nonlinear optical performance of two-dimensional MoS_2 nanofilms via defect engineering, *Nanoscale*, 2018, **10**, 17924–17931.
10 K. Kang, S. Xie, L. Huang, Y. Han, P. Y. Huang, K. F. Mak, C.-J. Kim, D. Muller and J. Park, High-mobility three-atom-thick semiconducting films with wafer-scale homogeneity, *Nature*, 2015, **520**, 656–660.
11 A.-P. Luo, M. Liu, X.-D. Wang, Q.-Y. Ning, W.-C. Xu and Z.-C. Luo, Few-layer MoS2-deposited microfiber as highly nonlinear photonic device for pulse shaping in a fiber laser, *Photonics Res.*, 2015, **3**, 69–78.
12 D. Li, W. Xiong, L. Jiang, Z. Xiao, H. R. Golgir, M. Wang, X. Huang, Y. Zhou, Z. Lin, J. Song, S. Ducharme, L. Jiang, J.-F. Silvain and Y. Lu, Multimodal nonlinear optical imaging of MoS_2 and MoS_2-based van der Waals Heterostructures, *ACS Nano*, 2016, **10**, 3766–3775.
13 X. Yin, Z. Ye, D. A. Chenet, Y. Ye, K. O'Brien, J. C. Hone and X. Zhang, Edge Nonlinear Optics on MoS_2 Atomic Monolayer, *Science*, 2014, **344**, 488–490.
14 Y. Yu, C. Li, Y. Liu, L. Su, Y. Zhang and L. Cao, Controlled Scalable Synthesis of Uniform, High-Quality Monolayer and Few-Layer MoS_2 Films, *Sci. Rep.*, 2013, **3**, 1–6.
15 K. Kang, S. Xie, L. Huang, Y. Han, P. Y. Huang, K. F. Mak, C. J. Kim, D. Muller and J. Park, High-Mobility Three-Atom-Thick Semiconducting Films with Wafer-Scale Homogeneity, *Nature*, 2015, **520**, 656–660.
16 Y. Zhan, Z. Liu, S. Najmaei, P. M. Ajayan and J. Lou, Large-Area Vapor-Phase Growth and Characterization of MoS_2 Atomic Layers on a SiO_2 Substrate, *Small*, 2012, **8**, 966–971.
17 N. Choudhary, J. Park, J. Y. Hwang and W. Choi, Growth of Large-Scale and Thickness-Modulated MoS_2 nanosheets, *ACS Appl. Mater. Interfaces*, 2014, **6**, 21215–21222.
18 X. Zhang, S. Zhang, B. Chen, H. Wang, K. Wu, Y. Chen, J. Fan, S. Qi, X. Cui, L. Zhang and J. Wang, Direct synthesis of large-scale hierarchical MoS2 films nanostructured with orthogonally orientated vertically and horizontally aligned layers, *Nanoscale*, 2016, **8**, 431–439.
19 Y.-H. Lee, X.-Q. Zhang, W. Zhang, M.-T. Chang, C.-T. Lin, K.-D. Chang, Y.-C. Yu, J. T.-W. Wang, C.-S. Chang, L.-J. Li and T.-W. Lin, Synthesis of Large-Area MoS_2 Atomic Layers with Chemical Vapor Deposition, *Adv. Mater.*, 2012, **24**, 2320–2325.
20 S. Najmaei, Z. Liu, W. Zhou, X. Zou, G. Shi, S. Lei, B. I. Yakobson, J. C. Idrobo, P. M. Ajayan and J. Lou, Vapour Phase Growth and Grain Boundary Structure of Molybdenum Disulphide Atomic Layers, *Nat. Mater.*, 2013, **12**, 754–759.
21 D. Kong, H. Wang, J. J. Cha, M. Pasta, K. J. Koski, J. Yao and Y. Cui, Synthesis of MoS_2 and $MoSe_2$ films with Vertically Aligned Layers, *Nano Lett.*, 2013, **13**, 1341–1347.
22 Y. Jung, J. Shen, Y. Liu, J. M. Woods, Y. Sun and J. J. Cha, Metal Seed Layer Thickness-Induced Transition from Vertical to Horizontal Growth of MoS_2 and WS_2, *Nano Lett.*, 2014, **14**, 6842–6849.
23 C. Stern, S. Grinvald, M. Kirshner, O. Sinai, M. Oksman, H. Alon, O. E. Meiron, M. Bar-Sadan, L. Houben and D. Naveh, Growth Mechanism and Electronic Properties of Vertically Aligned MoS_2, *Sci. Rep.*, 2018, **8**, 16480.
24 H. Wang, Z. Lu, S. Xu, D. Kong, J. J. Cha, G. Zheng, P.-S. Hsu, K. Yan, D. Bradshaw, F. B. Prinz and Y. Cui, Electrochemical Tuning of Vertically Aligned MoS_2 Nanofilms and Its Application in Improving Hydrogen Evolution Reactions, *Proc. Natl. Acad. Sci. U. S. A.*, 2013, **110**, 19701–19706.
25 R. Saito, Y. Tatsumi, S. Huang, X. Ling and M. S. Dresselhaus, Raman spectroscopy of transition metal dichalcogenides, *J. Phys.: Condens. Matter*, 2016, **28**, 353002–353018.
26 X. Zhang, X. F. Qiao, W. Shi, J. B. Wu, D. S. Jiang and P. H. Tan, Phonon and Raman Scattering of Two-Dimensional Transition Metal Dichalcogenides from Monolayer, Multilayer to Bulk Material, *Chem. Soc. Rev.*, 2015, **44**, 2757–2785.
27 H. Li, Q. Zhang, C. C. R. Yap, B. K. Tay, T. H. T. Edwin, A. Olivier and D. Baillargeat, From Bulk to Monolayer MoS_2: Evolution of Raman Scattering, *Adv. Funct. Mater.*, 2012, **22**, 1385–1390.
28 F. Moya, G. E. Moya-Gontier and F. Cabane-Brouty, Sulphur diffusion in copper: departure from the Arrhenius plot, *Phys. Status Solidi*, 1969, **35**, 893–901.
29 C. Stern, S. Grinvald, M. Kirshner, O. Sinai, M. Oksman, H. Alon, O. E. Meiron, M. Bar-Sadan, L. Houben and D. Naveh, Growth Mechanism and Electronic Properties of Vertically Aligned MoS_2, *Sci. Rep.*, 2018, **8**, 16480.
30 L. M. Malard, T. V. Alencar, A. P. M. Barboza, K. F. Mak and A. M. de Paula, Observation of intense second harmonic generation from MoS_2 atomic crystals, *Phys. Rev. B: Condens. Matter Mater. Phys.*, 2013, **87**, 201401–201406.
31 A. Säynätjoki, L. Karvonen, H. Rostami, A. Autere, S. Mehravar, A. Lombardo, R. A. Norwood, T. Hasan, N. Peyghambarian, H. Lipsanen, K. Kieu, A. C. Ferrari, M. Polini and Z. Sun, Ultra-strong nonlinear optical processes and triagonal warping in MoS_2 layers, *Nat. Commun.*, 2017, **8**, 893.
32 R. I. Woodward, R. T. Murray, C. F. Phelan, R. E. P. de Oliveira, T. H. Runcorn, E. J. R. Kelleher, S. Li, E. C. de Oliviera, G. J. M. Fechine, G. Eda and C. J. S. de Matos, Characterization of the second- and third-order nonlinear optical susceptibilities of monolayer MoS_2 using multiphoton microscopy, *2D Mater.*, 2016, **4**, 011006–011013.
33 R. W. Boyd, *Nonlinear optics*, Elsevier, 2013.
34 M. O. Cichocka, M. Bolhuis, S. E. van Heijst and S. Conesa-Boj, Robust Sample Preparation of Large-Area In- and Out-of-Plane Cross Sections of Layered Materials with Ultramicrotomy, *ACS Appl. Mater. Interfaces*, 2020, **12**, 15867–15874.